Neuropharmacology 208 (2022) 108985

Contents lists available at ScienceDirect

Neuropharmacology

journal homepage: www.elsevier.com/locate/neuropharm

In vivo imaging of alpha-synuclein with antibody-based PET

Sahar Roshanbin [a,*], Mengfei Xiong [a], Greta Hultqvist [b], Linda Söderberg [c], Olof Zachrisson [c], Silvio Meier [a], Sara Ekmark-Lewén [a], Joakim Bergström [a], Martin Ingelsson [a,d,e], Dag Sehlin [a], Stina Syvänen [a]

[a] Department of Public Health and Caring Sciences, Uppsala University, Uppsala, Sweden
[b] Department of Pharmaceutical Biosciences, Uppsala University, Uppsala, Sweden
[c] BioArctic, Stockholm, Sweden
[d] Krembil Brain Institute, University Health Network, Toronto, Ontario, Canada
[e] Department of Medicine and Tanz Centre for Research in Neurodegenerative Diseases, University of Toronto, Toronto, Canada

ARTICLE INFO

Keywords:
Positron emission tomography
Alpha-synuclein
Antibody radioligand
Neurodegeneration
Transgenic mice
L61

ABSTRACT

The protein alpha-synuclein (αSYN) plays a central role in synucleinopathies such as Parkinsons's disease (PD) and multiple system atrophy (MSA). Presently, there are no selective αSYN positron emission tomography (PET) radioligands that do not also show affinity to amyloid-beta (Aβ). We have previously shown that radiolabeled antibodies, engineered to enter the brain via the transferrin receptor (TfR), is a promising approach for PET imaging of intrabrain targets. In this study, we used this strategy to visualize αSYN in the living mouse brain. Five bispecific antibodies, binding to both the murine TfR and αSYN were generated and radiolabeled with iodine-125 or iodine-124. All bispecific antibodies bound to αSYN and mTfR before and after radiolabelling in an ELISA assay, and bound to brain sections prepared from αSYN overexpressing mice as well as human PD- and MSA subjects, but not control tissues in autoradiography. Brain concentrations of the bispecific antibodies were between 26 and 63 times higher than the unmodified IgG format 2 h post-injection, corresponding to about 1.5% of the injected dose per gram brain tissue. Additionally, intrastriatal αSYN fibrils were visualized with PET in an αSYN deposition mouse model with one of the bispecific antibodies, [^{124}I]RmAbSynO2-scFv8D3. However, PET images acquired in αSYN transgenic mice with verified brain pathology injected with [^{124}I]RmAbSynO2-scFv8D3 and [^{124}I]RmAb48-scFv8D3 showed no increase in antibody retention compared to WT mice. Despite successful imaging of deposited extracellular αSYN using a brain-penetrating antibody-based radioligand with no cross-specificity towards Aβ, this proof-of-concept study demonstrates challenges in imaging intracellular αSYN inclusions present in synucleinopathies.

1. Introduction

Misfolding and aggregation of alpha-synuclein (αSYN) is the common pathological hallmark of Parkinson's disease (PD), multiple system atrophy (MSA), dementia with Lewy bodies (DLB), and other α-synucleinopathies. These neurodegenerative disorders are characterized by a gradual loss of dopaminergic neurons leading to motor impairment, and in many cases also to cognitive decline (Salawu et al., 2010; Burn et al., 2006). In particular, accumulating evidence from *in vitro* and *in vivo* studies suggests that the oligomeric and protofibrillar forms of αSYN exhibit neurotoxic properties though a combination of different pathways (Ingelsson, 2016), including impairment of cell membrane integrity, synaptic toxicity and general cellular toxicity leading to increased loss of dopaminergic neurons (Winner et al., 2011; Danzer et al., 2007; Choi et al., 2013).

Brain dopamine function can be monitored and visualized by positron emission tomography (PET) or single photon emission computed tomography (SPECT) imaging. For example, a DaT or PE2I scan can be used to estimate the density of presynaptic dopamine reuptake transporters, which are indicative of the brain's dopaminergic function (Cummings et al., 2011; Appel et al., 2015) and will frequently show a decreased number of dopamine reuptake transporters in PD, DLB and MSA patients. However, it is likely that a change in dopaminergic function occurs at a later stage than the initiation of αSYN aggregation. In addition, other neurological conditions could also result in a

* Corresponding author. Department of Public Health and Caring Sciences, Uppsala University, Rudbecklaboratoriet, Dag Hammarskjöldsväg 20, 751 85, Uppsala, Sweden.
E-mail address: sahar.roshanbin@pubcare.uu.se (S. Roshanbin).

https://doi.org/10.1016/j.neuropharm.2022.108985
Received 4 July 2021; Received in revised form 5 January 2022; Accepted 2 February 2022
Available online 8 February 2022

Abbreviations

Aβ	amyloid-beta
αSYN	alpha-synuclein
MSA	multiple system atrophy
mTfR	murine transferrin receptor
PD	Parkinson's disease
PET	Positron Emission Tomography
TfR	transferrin receptor
Tg	transgenic
WT	wild-type

decreased density of dopamine transporters, such as Huntington's disease (Ginovart et al., 1997; Suzuki et al., 2001) and traumatic brain injury (Donnemiller et al., 2000; Jolly et al., 2019). Further, disease modifying treatments directed against αSYN are emerging, while existing treatments directed at boosting the dopaminergic transmission is regarded as a symptomatic relief that do not alter the underlying pathogenesis. Hence, to allow for early diagnosis and to investigate the effect of anti-αSYN treatments it would be valuable to visualize αSYN pathology rather than dopamine function. Unfortunately, there are currently no PET radioligands available for the selective visualization of αSYN, thus hampering both diagnostics of PD and the evaluation of possible disease modifying effects of novel drug candidates.

The development of PET-ligands for αSYN is focused primarily on small lipophilic molecules with fast pharmacokinetics that interact with intrabrain αSYN inclusions, in particular with the β-sheet structures of insoluble αSYN aggregates. Recently, radioligands with high *in vitro* affinity towards αSYN, have been described (Kuebler et al., 2020; Yu et al., 2012; Kikuchi et al., 2010). However, these radioligands also show some affinity towards aggregated amyloid-β (Aβ) fibrils, characteristic for Alzheimer's disease, as the β-sheet structures of aggregated αSYN and Aβ are similar (Kuebler et al., 2020; Heise et al., 2005; Fodero-Tavoletti et al., 2009). The coexistence of different types of brain pathology (αSYN, Aβ and tau) often observed in neurodegenerative diseases, in addition to differences in concentrations of the pathological proteins, requires highly selective markers (Clinton et al., 2010; Compta et al., 2011).

The specificity offered by antibodies could be one possible way to circumvent the problem with off-target binding. However, due to their size, passage across the blood-brain barrier (BBB) is very restricted. Consequently, brain distribution of antibodies is estimated to be less than 0.05% of the injected dose (Bard et al., 2000; Gustavsson et al., 2020; Syvänen et al., 2018; Sehlin et al., 2020; Hultqvist et al., 2017). Thus, to enable antibodies as PET-ligands their transport across the BBB must be facilitated.

In recent years, utilization of receptor-mediated transcytosis has been explored as a strategy to actively transport large proteins such as antibodies into the brain. In this respect, the transferrin receptor 1 (TfR), involved in iron transport to the brain, has been extensively studied, as it is highly expressed on the endothelial cells of the BBB (Niewoehner et al., 2014; Yu et al., 2011) as well as on neurons (Kariolis et al., 2020; Moos, 1996). Engineering antibodies into a bispecific format so that they, in addition to the primary target, also display affinity for the murine TfR1 (mTfR) can increase brain concentrations of full-sized IgG antibodies more than 50-fold in comparison with unmodified antibodies (Syvänen et al., 2018; Niewoehner et al., 2014; Yu et al., 2011, 2014; Syvanen et al., 2017). These brain concentrations, approximately 1% of the injected dose, are comparable to those observed with small lipophilic brain-penetrating drugs. The use of mTfR mediated transcytosis has been shown to be a successful concept in the development of antibody-based PET-ligands targeting Aβ (Sehlin et al., 2016, 2020; Syvanen et al., 2017; Fang et al., 2019) and the triggering receptor expressed on myeloid cells 2 (TREM2), a microglial marker (Meier et al., 2021). Bispecific antibodies thus present a promising possibility for visualization of intrabrain targets (Sehlin et al., 2019).

In the present study, we have designed five bispecific αSYN/mTfR antibodies, engineered to cross the BBB via mTfR-mediated transcytosis, and studied their ability to visualize αSYN *in vitro* and *in vivo* after radiolabeling. In an αSYN deposition model, we were able to successfully visualize extracellular αSYN with *in vivo* PET imaging. However, no specific PET signal was detected when imaging pathological αSYN in transgenic PD mouse models despite using a specific αSYN antibody as a PET ligand, demonstrating challenges in imaging intracellular targets.

2. Methods

2.1. Generation of recombinantly expressed antibodies targeting oligomeric/protofibrillar αSYN and mTfR

The recombinant αSYN/mTfR antibodies were designed as previously described for an Aβ directed antibody in the same bispecific format and linker (Hultqvist et al., 2017). In short, the antibodies were generated by fusion of a single-chain variable fragment (scFv) of 8D3 (Kissel et al., 1998), an antibody binding mTfR, to the C-terminal end of the light chain of an IgG2c backbone (Fig. 1). The αSYN IgG antibodies used were the following: RmAb48, RmAb38F, RmAb38E2, RmAb15 (Nordstrom et al., 2011; Fagerqvist et al., 2013) and RmAbSynO2 (Vaikath et al., 2015). RmAb48, RmAb38F, RmAb38E2, RmAb15 were all raised against 4-hydroxy-2-nonenal (HNE) stabilized human αSYN oligomers (Näsström et al., 2011), whereas RmAbSynO2 was generated by immunization with human αSYN fibrils. With the exception of RmAb15, that exhibits an equal affinity to monomers and oligomers, all αSYN antibodies show high affinity for larger oligomers and protofibrils. In addition, RmAbSynO2 has been shown to bind αSYN aggregates of varying sizes, from early oligomers to late fibrils (Vaikath et al., 2015).

All antibodies were expressed using a previously published protocol in Expi293 cells (A14527, ThermoFisher) (Fang et al., 2017). Briefly, cells were transiently transfected with a mix of pcDNA3.4 vectors carrying the sequence of either the heavy or the light chain of the antibody. Polyethylenimine (PEI) was used as transfection reagent and valproic acid (VPA) as a cell cycle inhibitor. The antibodies were purified using an ÄKTA system with a Protein G column (GE Healthcare AB, Uppsala, Sweden). Antibody integrity and functionality was assessed with ELISA and non-reduced SDS-page gel. Antibodies were mixed with Bolt® LDS 4x sample buffer and were loaded onto a 10% Bolt® Bis-Tris Plus Gel (both ThermoFisher) along with a Chameleon Li-Cor pre-stained protein ladder and run according to manufacturer's instructions. Gel was rinsed in dH_2O, stained with Page Blue (Fermentas) overnight and finally destained with dH_2O. All antibodies were expressed in both unmodified IgG and bispecific format for purposes of comparison.

2.2. Animals

In vitro autoradiography was performed on brain sections prepared from saline perfused Thy-1 αSYN mice (Line 61, "L61", age 5–7 months) overexpressing wild-type (WT) human αSYN (Chesselet et al., 2012; Rockenstein et al., 2002) on a B6D2F1/Crl background (n = 5) and age matched B6D2F1/Crl littermates (n = 5). L61 male mice display behavioral dysfunction and deposition of proteinase K-resistant and hyperphosphorylated αSYN pathology from 5 months of age (Chesselet et al., 2012; Roshanbin et al., 2021). All L61 mice included in the *in vitro* autoradiography were euthanized due to their severe motor phenotype.

Ex vivo studies of brain distribution of unmodified IgG and bispecific antibodies were performed in C57BL/6JBomTac mice (n = 30, age 11–12 months).

For *in vivo* PET imaging, we established an αSYN deposition model in which we deposited recombinant fibrils of αSYN in the striatum of B6D2F1/Crl WT mice (see supplementary materials and methods) for *in*

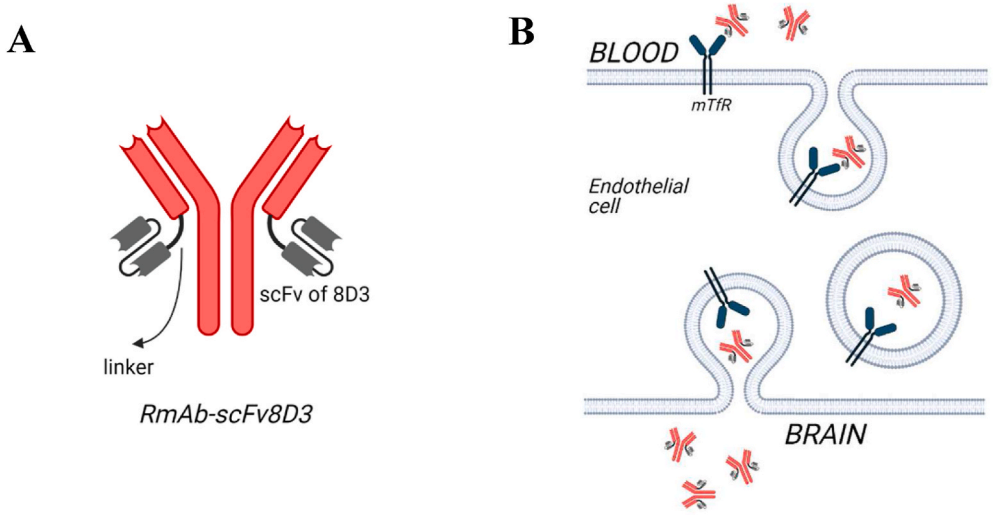

Fig. 1. A) Design of the bispecific antibodies expressed targeting αSYN, with the short linkers between the C-terminus and the scFv8D3. B) Active transport of the bispecific αSYN antibody across the BBB through mTfR-mediated transcytosis.

vivo and *ex vivo* evaluation of the bispecific antibodies (n = 11 fibril injected and n = 5 PBS injected, all 5–7 months). The αSYN fibrils were unsonicated to reduce cell internalization and clearance of the fibrils prior to imaging (suppl. Figure 1) (Karpowicz et al., 2017) and validated *ex vivo* between 5 and 12 days post-intracranial injection.

In addition to the above-mentioned model, the L61 mice and B6D2F1/Crl controls (n = 5 and n = 4 respectively, all aged 11–12 months) were used for PET imaging, as well as a second αSYN model, the (Thy-1)-h[A30P] (A30P) line expressing human αSYN with the A30P-mutation on a C57BL/6J background (n = 3, aged 18–22 months) (Ekmark-Lewén et al., 2018; Kahle et al., 2000).

All animal procedures complied with the ARRIVE guidelines and were carried out in accordance with the European Communities Council Directive of September 22, 2010 (2010/63/EU) and were approved by the Uppsala County Animal Ethics Board (#5.8.18–13350/2017) and Stockholm North Animal Research Ethical Board (5789–2018). A summary of mice included in the study is displayed in Supplementary Table 1.

2.3. Human brain

Human *post-mortem* tissue was obtained from the Netherlands Brain Bank (NBB, Netherlands Institute for Neuroscience, Amsterdam). All tissue samples were collected from donors from whom written consent for brain autopsy had been obtained prior to death. MSA, PD and AD patients were clinically and neuropathologically diagnosed according to current guidelines and further confirmed by immunohistochemistry (see supplementary information). In addition, age-matched controls without signs of neurological disease or αSYN or Aβ pathology were included. Demographic data of the cases are listed in Supplementary Table 2.

2.4. Biochemical analyses

Assessment of binding properties of the bispecific and unmodified antibodies to oligomeric αSYN and mTfR *in vitro* before and after radiolabeling was performed using direct ELISA. The 96-well plates (Corning Inc., Corning, NY, USA) were coated with either 25 ng/well mTfR or 50 ng/well HNE-induced αSYN oligomers diluted in PBS over night at +4 °C. The following day, plates were decanted and blocked for 1 h with 1% BSA in PBS prior to incubation with serially diluted antibodies for 2 h. Bound antibodies were detected by incubation with HRP-conjugated 1:2000 diluted anti-mouse-IgG-F(ab')$_2$ (115-036-006, Jackson ImmunoResearch Laboratories, West Grove, PA, USA) for 1 h. Signals were developed using K blue aqueous TMB substrate (Neogen Corp., Lexington, KY, USA) and read with a spectrophotometer at 450 nm. Wells were washed three times in ELISA-washing buffer (phosphate-buffered NaCl with 0.1% Tween 20 and 0.15% ProClin, all Sigma Aldrich, Stockholm, Sweden) between each step of the ELISA. All antibody dilutions were made in ELISA incubation buffer (PBS with 0.1% BSA, 0.05% Tween, and 0.15% ProClin), and all incubations took place in room temperature on a shaker at 900 rpm.

2.5. Radiochemistry

The antibodies were labeled with iodine-125 (^{125}I) for *in vitro* autoradiography and brain distribution studies, and with iodine-124 (^{124}I) for imaging with PET and subsequent *ex vivo* autoradiography. The labeling was performed using direct iodination with Chloramine-T (Syvänen et al., 2018) as previously described for ^{125}I (Gustavsson et al., 2020) and ^{124}I (Meier et al., 2018). The radiolabeling was always performed less than 2 h before the experiments, and the yield calculation was based on the amount of radioactivity added and the activity of the obtained purified antibody. [^{11}C]PIB (Pittsburgh compound B) was produced as previously described (Klunk et al., 2004).

Molar activity for all radioligands used for autoradiography and brain distribution studies are summarized in Supplementary Tables 3 and 4, respectively. All antibodies were spun at 20 000×*g* for 10 min prior to injection to avoid major aggregates.

2.6. Autoradiography

For *in vitro* autoradiography, 20 μm unfixed cryo sections were incubated overnight at 4 °C with 0.2 μg/mL of ^{125}I-labeled antibody in both the bispecific and unmodified IgG format, either on their own or co-incubated with 100-fold unlabeled antibody or with 50xK_D of the 8D3 antibody (K_D = 2.3 nmol, (Boado et al., 2009)), blocking the transferrin receptor. The next day, all sections were washed (3 × 15 min PBS and dH_2O for 30 s) and dried before exposure to positron-sensitive phosphor screens (MS, MultiSensitive, PerkinElmer, Downers grove, IL, USA) for 24 h. The phosphor screens were scanned in a Cyclone Plus Imager system (PerkinElmer) at a resolution of 600 dots per inch and converted to a false color scale (Royal) using ImageJ.

Unfixed 8 μm cryo sections were prepared from MSA putamen and PD (Braak stage 6) substantia nigra. As controls, sections from respective brain regions from age-matched non-neurological elderly controls were used. In addition, sections from an AD subject (Braak stage 6, superior

occipital gyrus) as well as a control subject were prepared and included in the analyses. Sections were incubated overnight with 0.2 μg/mL of [^{125}I]RmAb48-scFv8D3 or [^{125}I]RmAbSynO2-scFv8D3 at 4 °C, either in radioligand only or co-incubated with 100-fold excess of unlabeled antibody. Sections were washed, dried as previously described, and exposed to phosphor screens for 1 h in RT. Screens were scanned in a Typhoon phosphorimager (GE Healthcare) and converted to a false color scale (Royal) using ImageJ.

For *ex vivo* autoradiography, 20 μm unfixed cryo sections were exposed to phosphor screens and scanned as described above for *in vitro* autoradiography mouse sections.

2.7. Brain distribution

Mice received intravenously (i.v.) administered trace doses of 0.05 mg/kg ^{125}I-labeled antibodies, followed by a terminal blood sample from the heart prior to the transcardial perfusion 2 h post-injection. Radioactivity levels in perfused brains and blood samples were measured with a γ-counter (1480 Wizard™, Wallac Oy, Turku, Finland). Based on the measured radioactivity, antibody concentrations were quantified as percent of injected dose per gram tissue (%ID/g).

2.8. Validation of radioligand binding

For further validation of the model, a blocking experiment was performed in which fibril deposition model mice were intravenously administered 20 mg/kg unlabeled RmAbSynO2-scFv8D3 (n = 2) or PBS (n = 2) seven days following the intracranial αSYN fibril injections. Three days later, mice were administered 0.05 mg/kg of [^{125}I]RmAbSynO2-scFv8D3. Antibody stability in plasma was investigated with instant thin-layer chromatography (iTLC, see supplementary materials and methods). Mice were perfused three days after the radioligand injections. Brains were flash-frozen and sectioned for further analysis.

2.9. Thioflavin-S staining

For visualization of the injected fibrils in 20 μm cryo sections from the αSYN deposition model, slides were incubated in 1% aqueous Thioflavin-S (Sigma Aldrich, Stockholm, Sweden) for 8 min at room temperature. Slides were subsequently washed in an increasing percentage of ethanol; 2 × 3 minutes in 70, 95 and 99.9% ethanol, followed by mounting in DPX mounting medium and dried overnight. Fluorescent images were acquired using the Observer Z1 microscope (Zeiss, Jena, Germany). Incubation, washing and drying of sections all took place in darkness due to light sensitivity of the Thioflavin-S.

2.10. PET studies

All mice included in PET studies received drinking water supplemented with 0.2% iodine to reduce thyroidal uptake of ^{124}I throughout the study, starting the day before the radioligand administration. Animals were injected with either 11 ± 0.5 MBq [^{124}I]RmAbSynO2 (n = 3), 10.2 ± 0.3 MBq [^{124}I]RmAbSynO2-ScFv8D3 (n = 10) or 16 ± 0.7 MBq [^{124}I]RmAb48-ScFv8D3 (n = 10), at a dose of 0.5 mg/kg. The molar activities for the radioligands were 192 MBq/nmol for [^{124}I]RmAbSynO2-scFv8D3, 121.5 MBq/nmol for [^{124}I]RmAbSynO2-scFv8D3 and 220 MBq/nmol for [^{124}I]RmAb48-scFv8D3. Antibody injections took place 48–96 h prior to scanning to ensure sufficient signal-to-noise ratio after clearance of the radioligand from the blood as demonstrated by previous pharmacokinetic studies in both WT and transgenic AD animals (Gustavsson et al., 2020; Sehlin et al., 2019; Faresjö et al., 2021). To monitor the blood concentration of the radioligand, blood samples (8 μl) were obtained at 1, 3, 6, 24, 48, 72, and 96 h post-injection, including a terminal blood sample prior to transcardial perfusion with saline. To further verify the presence of fibrils in the αSYN deposition model, mice were scanned with [^{11}C]PIB, shown to bind to αSYN fibrils (Fodero-Tavoletti et al., 2007; Ye et al., 2008). Mice (n = 4) were injected with 10.3 ± 5 MBq at scan start, with a molar activity of 138 MBq/nmol. All molar activities were measured at the end of labeling, and injections were performed within 2 h of labeling.

Mice were anesthetized with 1.8–1.2% isoflurane, placed in the gantry of a small animal PET/Computed Tomography (CT) scanner (Triumph Trimodality System, TriFoil Imaging, Inc., Northridge, CA, USA) and scanned for 60 min in list mode for both antibody PET and [^{11}C]PIB PET. PET scans were followed by a CT examination for 3 min (field of view = 8.0 cm), as previously described (Sehlin et al., 2016; Hultqvist et al., 2017). After the scan, mice were euthanized through cardiac puncture followed by transcardial perfusion.

PET data was reconstructed using a maximum likelihood expectation maximization (MLEM) two-dimensional algorithm (10 iterations). The CT raw files were reconstructed using filter back projection. All subsequent processing of the PET and CT images were performed in imaging software Amide 1.0.4. The CT scan was manually aligned with a T2-weighted, magnetic resonance imaging-based mouse brain atlas containing outlined regions of interests for hippocampus, striatum, thalamus, cortex and cerebellum. The PET image was aligned with the CT and, thus, the magnetic resonance imaging atlas was also aligned with the PET data. The PET data was quantified as a concentration ratio of the radioactivity in five regions of interest (whole brain, cortex, hippocampus, thalamus and striatum) to that in cerebellum. Levels of radioactivity in the blood and different brain regions were measured with a well counter as previously described.

2.11. Image analysis

Radioactive signal on sections from fibril deposition model mice subject to injections of unlabeled RmAbSynO2-scFv8D3 or PBS prior to administration of radioligand were analyzed using ImageJ. Scanned images were converted to a false color scale (Royal) in ImageJ, whereafter an average of the integrated density of the fibril spot was obtained with same-sized ROIs on 12 sections per mouse.

2.12. Statistical analyses

Data were analyzed in GraphPad Prism version 9.0.0 for Windows (GraphPad Software, San Diego, USA). Comparison of bispecific and unmodified antibody brain delivery was investigated with a paired *t*-test. Results are reported as mean ± SD. Significance was set to 95% and indicated as *: $p < 0.05$, **: $p < 0.01$, ***: $p < 0.001$, ns: $p > 0.05$.

3. Results

3.1. Generation of bispecific αSYN antibodies and validation of in vitro binding properties to αSYN and mTfR

Unmodified antibodies were produced in yields of 20–25 mg/L transfection medium, while bispecific antibodies were produced in yields between 10 and 16 mg/L transfection medium, with assumed molecular weights of 150 and approximately 205 kDa respectively. Antibody size and purity was assessed with SDS-PAGE under non-reducing conditions (Fig. 2A, full untruncated image in suppl. Figure 2). For the unmodified antibody, a single band at 160 kDa was observed, and for the bispecific antibody at 250 kDa due to its bulkiness, showing that the products were pure and homogenous. Binding properties of the αSYN antibodies in their unmodified and bispecific formats were evaluated with indirect ELISA (Fig. 2). All antibodies exhibited a similar binding profile to αSYN oligomers in their unmodified and bispecific format. Unspecific binding to mTfR was low for the unmodified antibodies as expected, whereas the bispecific antibodies differed somewhat in their mTfR affinity. Labeling yield of the antibodies was approximately 70% for both ^{125}I and ^{124}I. Evaluation of *in vitro* binding properties with ELISA after labeling showed a somewhat reduced

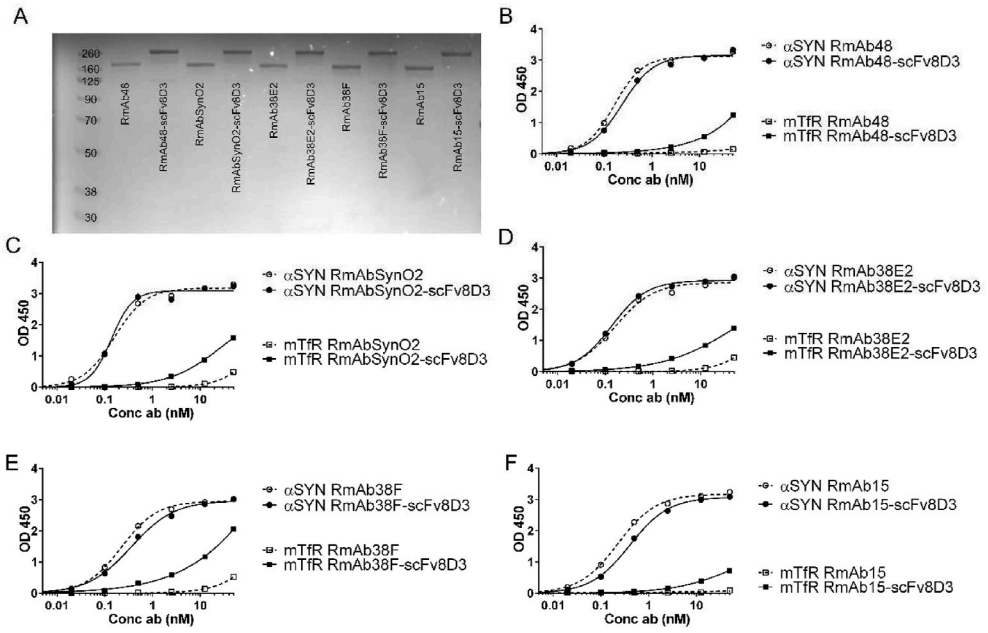

Fig. 2. A) SDS-PAGE gel displaying the bispecific antibodies and their unmodified variants. Bispecific antibodies generate a single band around 250 kDa, whereas the unmodified IgGs are displayed around 160 kDa. *In vitro* binding profile of the different bispecific antibodies to αSYN oligomers/protofibrils (circles) and mTfR (squares) in comparison with the unmodified antibodies using direct ELISA. Binding to αSYN is similar in both formats, with low unspecific binding to the mTfR in the unmodified format for RmAb48 (B), RmAbSynO2 (C), RmAb38E2 (D), RmAb38F (E) and RmAb15 (F). Graphs are representative.

binding affinity to mTfR whereas binding to αSYN remained largely unaffected (suppl. Figure 3).

3.2. *In vitro* autoradiography on pathological αSYN tissue

The αSYN antibodies, both unmodified and bispecific, bound more pronouncedly to L61 brain sections compared to sections prepared from B6D2F1 WT littermates (Fig. 3). The difference in bispecific antibody

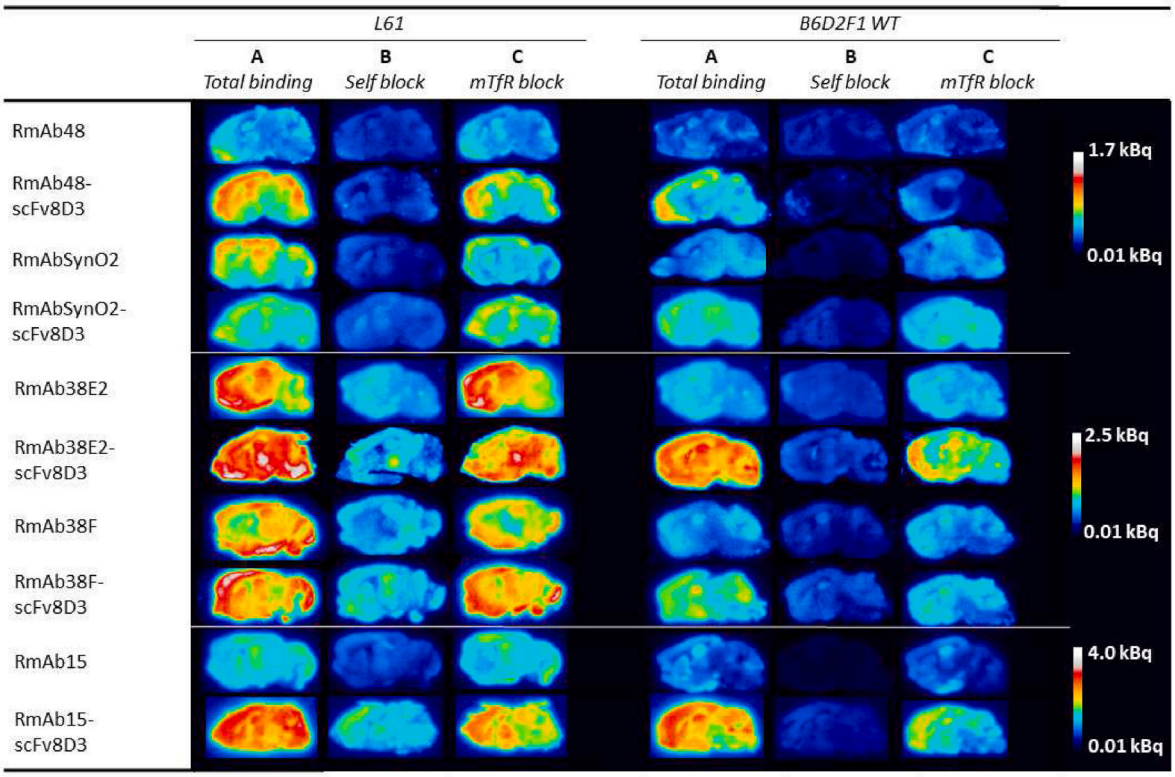

Fig. 3. *In vitro* autoradiography with αSYN antibodies on pathological L61 mouse brain sections. Bispecific ^{125}I-labeled antibodies targeting αSYN and the mTfR as well as unmodified variants of RmAb48, RmAbSynO2, RmAb38E2, RmAb38F and RmAb15 were evaluated on 20 μM cryo sections from L61 male mice between 5 and 7 months (left) and B6D2F1 WT controls (right). Comparisons can only be made within each row, representing one antibody. Antibodies have been further subdivided into three groups depending on the scaling. The A columns represent sections incubated with bispecific ^{125}I-labeled antibodies, and the B columns represents sections co-incubation with a 100-fold excess of cold, unlabeled antibody. In the C columns, the binding to mTfR was blocked by using 50x K_D of the 8D3 antibody binding to mTfR, representing the binding to αSYN only. Images are representative.

binding between L61 and WT became more evident when sections were co-incubated with a 100-fold excess of the cold, unlabeled bispecific antibody. The reduced signal in L61 after co-incubation indicated specific binding to αSYN. Sections incubated with bispecific antibody and 8D3, at a concentration 50-fold higher than the K_D for 8D3, reduced the signal somewhat, especially for the B6D2F1 WT sections, indicating that some of the signal was derived from bispecific antibody binding to mTfR rather than to αSYN.

Two antibodies, RmAb48-scFv8D3 and RmAbSynO2-scFv8D3, were chosen for further evaluation of binding to patient-derived αSYN on human tissue, as they exhibited the highest selectivity for aggregates over monomers (Nordstrom et al., 2011; Vaikath et al., 2015). The bispecific antibodies bound to a greater extent to cryo sections of putamen from an MSA patient in comparison with putamen from a control subject (Fig. 4). The specificity of this binding was validated by co-incubating the putamen sections with 100-fold excess of cold, unlabeled antibody, which almost completely blocked the signal. The same held true for substantia nigra from a PD-patient, exhibiting a more pronounced signal in comparison to the same brain region in a control subject. Also here, 100-fold excess of the unlabeled antibodies blocked the signal. To verify the specificity for αSYN over Aβ, brain sections from an AD patient was included, and binding of the antibodies to these sections were similar to that of control tissue, and homologous blocking with 100-fold excess of the unlabeled antibodies did not alter the signal. Presence of αSYN and Aβ on the sections was further verified with immunohistochemistry (suppl. Figure 4).

3.3. Increased brain uptake of bispecific antibodies targeting αSYN and mTfR

To assess the *in vivo* functionality of the bispecific antibodies, mice were administered tracer doses (~0.05 mg/kg) of ^{125}I-labeled antibodies. The brain concentration of the bispecific antibody at 2 h after i.v. administration was significantly higher than that for the unmodified antibody for all five studied antibody pairs (Fig. 5). The brain concentrations of the unmodified antibodies ranged from 0.02 to 0.04% ID/g brain, while the average brain concentrations of the bispecific antibodies ranged between 1.1 and 1.6% ID/g brain. Thus, bispecific modification resulted in slightly different relative brain concentration increases; the smallest was found for RmAb48 (26-fold) and the highest for RmAb38F (63-fold).

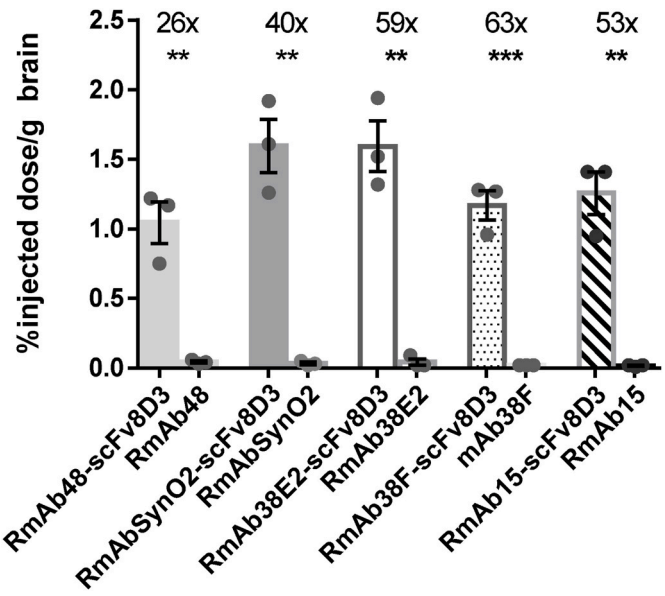

Fig. 5. Increased brain uptake of bispecific αSYN antibodies compared to their unmodified variants. Calculation of relative increase, based on the brain uptake of the antibody in the unmodified format, ranged between 26- to 63-fold. An independent, unpaired, two-tailed Student's t-test was used for comparison of the percentage uptake in the brain between the bispecific antibody and the unmodified variant (RmAb48-scFv8D3: $p = 0.0026$; RmAbSynO2-scFv8D3: $p = 0.0012$; RmAb38E2-scFv8D3: $p = 0.011$; RmAb38F-scFv8D3: $p = 0.0004$; RmAb15-scFv8D3: $p = 0.0013$).

3.4. In vivo PET-imaging of αSYN fibrils with [^{124}I]RmAbSynO2-ScFv8D3 in an αSYN deposition model

RmAbSynO2-ScFv8D3 labeled with ^{124}I was also evaluated as a PET-ligand in an αSYN deposition model developed for ensuring the availability of the pathological proteins. The deposition model was established by intrastriatal stereotaxic injection of unsonicated pre-formed αSYN-fibrils. The model was validated by *ex vivo* autoradiography, in which the striatal αSYN deposition was visible in mice injected with [^{125}I]RmAbSynO2-scFv8D3, whereas no signal was observed when injected with [^{125}I]RmAbSynO2 (Fig. 6A). Neither of the antibodies generated a signal in mice that had received an intrastriatal PBS deposition. To further validate the *in vivo* binding of [^{125}I]RmAbSynO2-

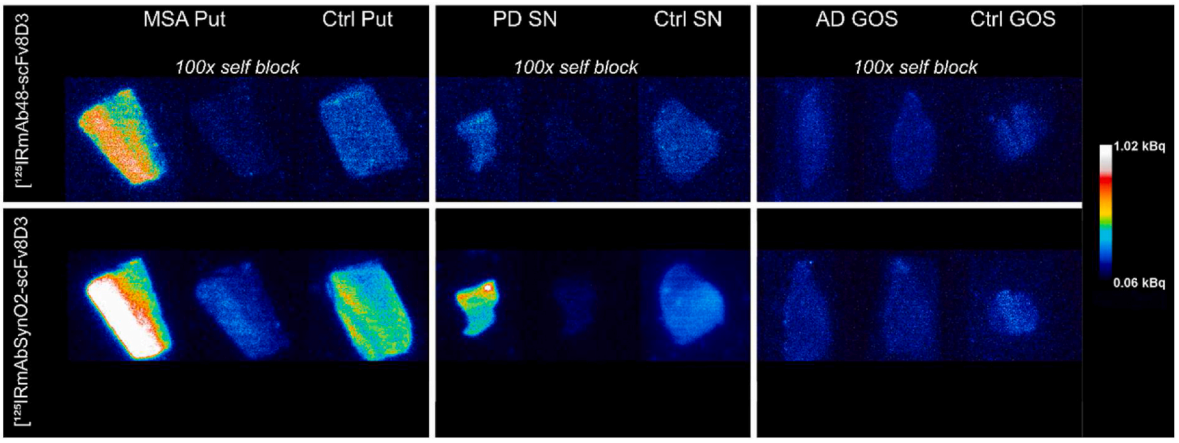

Fig. 4. *In vitro* autoradiography with bispecific [^{125}I]RmAb48-scFv8D3 and [^{125}I]RmAbSynO2-scFv8D3 on human MSA, PD and AD brain sections. Both bispecific antibodies showed a higher degree of binding to αSYN in MSA tissue from the putamen (Put, Braak LB unknown) and PD tissue from substantia nigra (SN, Braak LB stage 6) in comparison with tissue from respective brain regions from controls. Binding of antibodies to AD tissue from superior occipital gyrus (GOS) with Aβ pathology (Braak stage 6) was comparable to that of the control sections from the same region in control subjects. The signal was blocked with a 100-fold concentration of the unlabeled antibodies on both MSA and PD tissue, whereas the self-blocking in AD sections did not alter the signal.

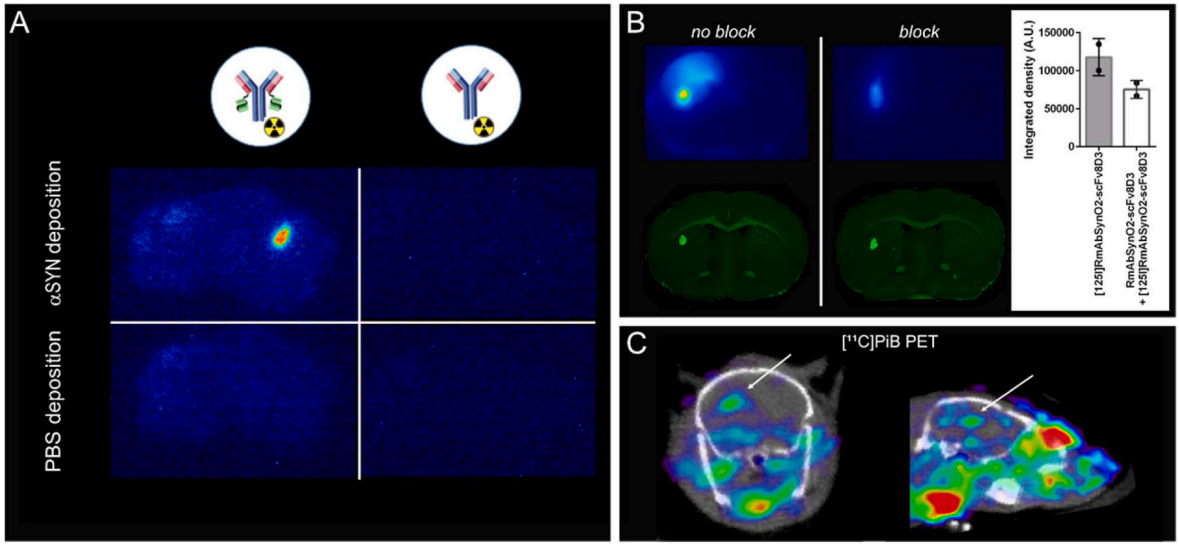

Fig. 6. A) Representative e*x vivo* autoradiography images of sagittal brain section from mice with striatal αSYN deposition and control mice with striatal PBS deposition injected with either [^{125}I]RmAbSynO2-scFv8D3 (left column) or [^{125}I]RmAbSynO2 (right column). αSYN deposition model mice exhibit a high intensity spot corresponding to the injection site when injected with [^{125}I]RmAbSynO2-scFv8D3, but not when injected with [^{125}I]RmAbSynO2. In contrast, no signal was observed with either antibody after striatal PBS deposition. B) Representative *ex vivo* autoradiography images of coronal brain sections from deposition model mice subject to blocking with unlabeled RmAbSynO2-scFv8D3 (top right) or PBS (top left) three days prior to administration of [^{125}I]RmAbSynO2-scFv8D3. For mice only receiving [^{125}I]RmAbSynO2-scFv8D3, density values were 117 776 ± 24 480 (n = 2), whereas values for mice receiving an injection of unlabeled RmAbSynO2-scFv8D3 prior to [^{125}I]RmAbSynO2-scFv8D3 injection were 75 496 ± 12 011 (n = 2), indicating a lowering of the signal originating from the fibril spot. Values are presented as mean ± SD. Fluorescent images of Thioflavin-S (ThS) bound to αSYN fibrils in the striatum from adjacent sections are displayed below, verifying presence of fibrils. C) Representative [^{11}C]PIB PET images (average signal 40–60 min post injection) of αSYN deposition model, showing brain retention in the striatum corresponding to the fibril injection site 5 days following fibril injection.

scFv8D3 to the deposited αSYN, a blocking experiment with cold antibody was performed. Quantified *ex vivo* radioactivity originating from the fibril deposition spot on brain sections indicated a 35% lower signal in mice that received injections of cold antibody prior to radioligand administration in comparison with mice that only received the radioligand. In addition, [^{125}I]RmAbSynO2-scFv8D3 displayed high stability with approximately 95% intact antibody between 1 and 72 h after injection (suppl. Figure 5). The presence of αSYN fibrils was also verified by *in vivo* [^{11}C]PIB PET that revealed radioligand retention in a spot corresponding to the injection site (Fig. 6C).

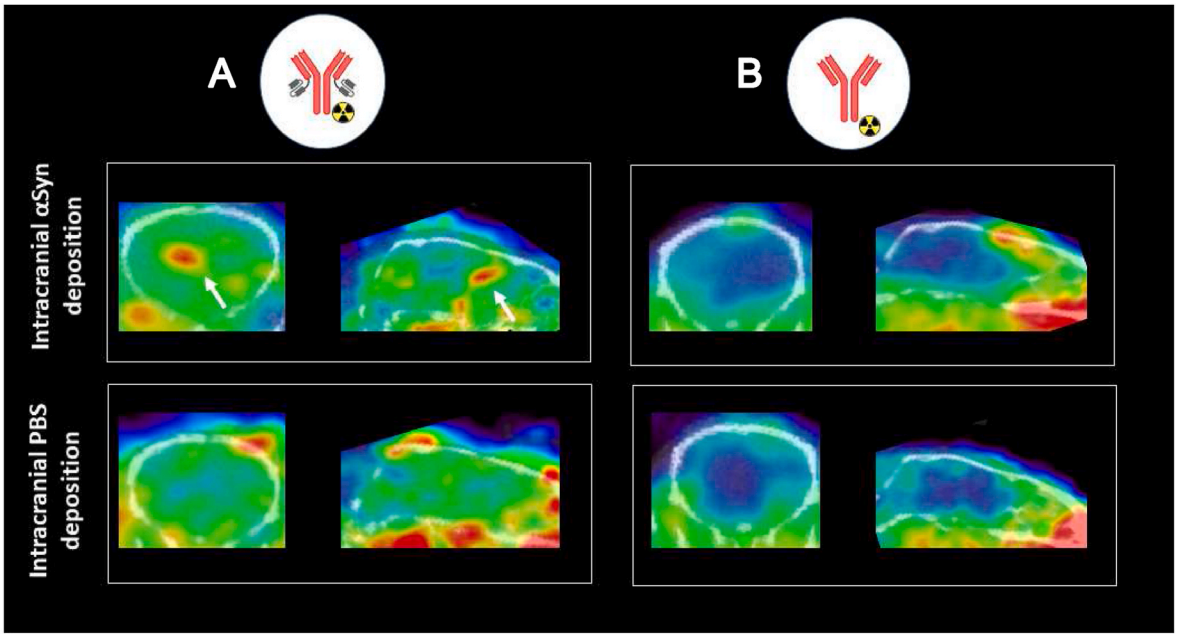

Fig. 7. Representative PET images obtained during a 60 min scan showing the coronal (left columns) and sagittal (right columns) views of B6D2F1 WT mice stereotactically injected in the striatum with either αSYN fibrils or PBS 7–8 days prior to radioligand administration. A) Only animals with αSYN deposition scanned with the bispecific antibody showed a positive PET signal corresponding to the injection site (arrows). PBS-injected mice scanned with the bispecific antibody displayed a high general brain distribution but no retention around the injection site. B) Animals scanned with the unmodified antibody exhibited a limited signal in the brain, and no retention associated with the injection site in neither αSYN deposition model mice nor PBS-injected mice.

Next, αSYN deposition model mice as well as control mice injected with PBS in the striatum were PET scanned with [^{124}I]RmAbSynO2-ScFv8D3 and [^{124}I]RmAbSynO2. The deposited αSYN was clearly visible as a high intensity spot indicating *in vivo* binding, while mice with intrastriatal PBS injections showed no such signal with the same antibody (Fig. 7A) despite exhibiting a high general brain distribution. In addition, animals administered with unmodified [^{124}I]RmAbSynO2 displayed no brain PET signal corresponding to the injection site, regardless of deposition material (Fig. 7B), indicating BBB integrity is not compromised by the deposition. PET/CT images superimposed with a T2-weighted MRI atlas is provided as Supplementary Fig. 6.

3.5. *In vivo PET imaging with [^{124}I]RmAb48-scFv8D3 and [^{124}I]RmAbSynO2-scFv8D3 in L61 and A30P mice*

Next, RmAb48-scFv8D3 and RmAbSynO2 were assessed as PET ligands for detection of αSYN *in vivo* in the L61 and A30P mouse models. Mice were PET-scanned during 60 min at 72 h post i.v. injection of either [^{124}I]RmAb48-scFv8D3 or [^{124}I]RmAbSynO2-scFv8D3. No differences were observed in the brains of L61 and A30P mice when comparing with WT controls (Fig. 8A) when scanning with either of the bispecific antibodies. To verify the presence of pathology in the animals included in the PET scan, αSYN levels from different regions were analyzed with Meso Scale Disocvery (MSD, suppl. Figure 7). The half-life of the antibodies, as calculated by the measured radioactivity in blood between 3 h and 3 days post injection, was similar between the mouse models. [^{124}I]RmAb48-scFv8D3 half-life was 18.9 ± 2.2 h in L61 mice, 15.6 ± 1.7 h in A30P mice and 17 ± 0.7 h in WT mice. [^{124}I]RmAbSynO2-scFv8D3 half-life was 24.7 h in L61 mice, 22.6 h in A30P mice and 21 h in WT mice (Fig. 8B). PET data were quantified as the concentration of [^{124}I]RmAb48-scFv8D3 and [^{124}I]RmAbSynO2-scFv8D3 in the whole brain and 8 subregions (hippocampus, thalamus, caudate nucleus, cortex, olfactory bulb, hindbrain and brainstem) relative to the concentration in cerebellum. All analyzed regions displayed low levels of respective PET ligand, with no difference between the L61 and A30P animals compared to controls (suppl. Figure 8).

4. Discussion

The implementation of molecular imaging in the past 20 years has broadened our understanding of PD and refined the diagnostic procedure. Available radioligands for PD diagnosis are focused on the dopaminergic system or changes in brain metabolism. A key event in the pathophysiology of PD is the abnormal aggregation of αSYN into fibrillar inclusions, with involvement of more and more brain regions as the disease progresses, distinguishing PD from other disorders with similar symptoms. Therefore, assessment of the extent and distribution pattern of αSYN pathology *in vivo* would be a highly valuable tool for diagnosis, disease staging and for the evaluation of target-site effects of novel drug candidates.

In the present study, we present an antibody-based strategy for imaging of aggregated αSYN *in vivo* using a bivalent mTfR shuttle format previously described for RmAb158-scFv8D3, a PET radioligand for the visualization of Aβ (Hultqvist et al., 2017). This format results in a highly efficient brain distribution, and was here generalized to antibodies targeting αSYN. *In vitro* evaluation of the antibodies revealed that binding to αSYN oligomers and mTfR remained stabile after antibody engineering and radiolabeling. As compromised specificity has been the main challenge in the development of PET radioligands for αSYN, we used autoradiography to validate the specificity by screening the five bispecific antibodies using brain sections prepared from L61 mice expressing human αSYN, on which a high, specific binding was noted in comparison with B6D2F1 WT controls. We also examined the contribution of the mTfR binding to the signal by blocking the mTfR sites with an excess of 8D3, an mTfR antibody (Kissel et al., 1998), showing that the autoradiography signal mainly was derived from the αSYN binding.

To demonstrate the translatability from the preclinical situation to the clinic, we showed specific binding of the two antibodies with the highest selectivity towards larger aggregated species over monomers, [^{125}I]RmAb48-scFv8D3 and [^{125}I]RmAbSynO2-scFv8D3, to αSYN on brain tissue sections from MSA and PD subjects, but not on sections from healthy control subjects. In addition, neither antibody showed specific binding to Aβ on section from AD subjects, verifying the selectivity of the antibodies to αSYN over Aβ in brain tissue. This is highly desirable as αSYN pathology frequently is concomitant with Aβ pathology (Alafuzoff and Libard, 2020; Robinson et al., 2018; Irwin et al., 2017).

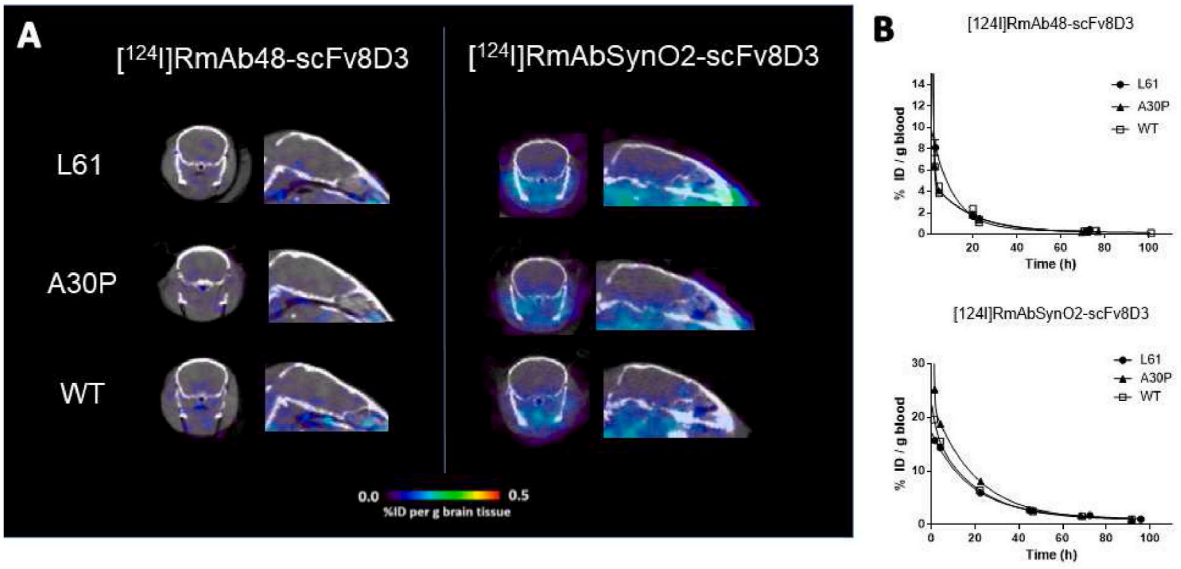

Fig. 8. A) Representative PET images obtained during a 60 min scan 72 h post-injection of [^{124}I]RmAb48-scFv8D3 (left) and [^{124}I]RmAbSynO2-scFv8D3 (right) in L61, A30P and B6D2F1 WT, all displaying low brain retention of the radioligand. B) Similar blood pharmacokinetics of the bispecific antibodies between groups; [124I]RmAb48-scFv8D3 half-life was 18.9 ± 2.2 h in L61 mice, 15.6 ± 1.7 h in A30P mice and 17 ± 0.7 h in WT mice, whereas [124I]RmAbSynO2-scFv8D3 half-life was 24.7 h in L61 mice, 22.6 h in A30P mice and 21 h in WT mice.

In vivo validation of the bispecific antibodies demonstrated high brain delivery resulting in brain concentrations of 1.1–1.6% ID/g. This is substantially higher than what was measured for the unmodified antibodies that displayed brain concentrations between 0.02 and 0.04 %ID/g. The brain concentrations were also similar to those published for RmAb158-scFv8D3, i.e. an antibody expressed in the same bispecific format (Syvänen et al., 2018; Hultqvist et al., 2017). In an αSYN fibril deposition model, the fibrils were visualized as a clear high intensity spot corresponding to the injection site when scanned with [^{124}I]RmAbSynO2-scFv8D3, whereas no signal was visible when scanning with [^{124}I]RmAbSynO2, indicating BBB integrity following the intracranial injections. Similarly, in control mice with intrastriatal PBS-injections, no signal was observed when scanning with either antibody. In addition, *in vivo* binding of [^{125}I]RmAbSynO2-scFv8D3 to the αSYN fibrils was reduced after pre-administration of cold RmAbSynO2-scFv8D3 indicating specific binding to the target. The presence of fibrillar αSYN was further verified by staining with ThS as well as scanning with [^{11}C]PIB, that has previously been shown to bind to αSYN fibrils *in vitro*, albeit with lower affinity than to Aβ (Foder-o-Tavoletti et al., 2007; Ye et al., 2008). These experiments demonstrate the ability of the bispecific radioligand [^{124}I]RmAbSynO2-scFv8D3 to bind and visualize αSYN *in vivo*. Still, we were not able to detect a PET signal *in vivo* in transgenic L61 or A30P mice, following administration of [^{124}I]RmAb48-scFv8D3 and [^{124}I]RmAbSynO2-scFv8D3, despite high brain concentrations of the antibodies and the presence of high levels of pathological αSYN in the brain of the scanned animals.

The positive PET signal in the αSYN deposition model and the *in vitro* characterization of the antibodies showed that the antibodies displayed a high sensitivity towards aggregated αSYN. Therefore, we speculate that the lack of signal in the L61 and A30P mice primarily relates to the intracellular localization of the target (Chesselet et al., 2012; Kahle et al., 2000; Spillantini et al., 1997; Lashuel et al., 2013). Although there are mechanisms by which antibodies are transported into cells to access intracellular αSYN deposits, e.g. via transferrin receptors expressed on neurons (Kariolis et al., 2020; Moos, 1996), it may be difficult to image these intracellular deposits with iodine labeled radioligands. Iodine is a non-residualizing nuclide that will be rapidly cleared from the cell after antibody internalization and subsequent lysosomal degradation. An alternative would be to use intracellularly trapped radiometals such as zirconium-89 or copper-64 for radiolabeling.

In addition, the overall low levels of αSYN in the brain in comparison with Aβ poses a challenge in αSYN tracer development (Shah et al., 2014; Deramecourt et al., 2006).

5. Conclusion

In summary, we have presented a novel approach for *in* vivo imaging of αSYN using an antibody-based PET tracer, with recombinantly expressed bispecific antibodies as an alternative to radioligands based on small molecules that often display affinity also to other aggregated proteins. We performed extensive *in vitro* validation to pathological αSYN and *in vivo* validation with significantly increased brain concentrations as well as imaging of αSYN fibrils deposited in the living mouse brain. However, as the pathological αSYN in the transgenic mouse lines could not be visualized with PET, this study further demonstrates that αSYN PET radioligands need to cross additional barriers to reach intracellular targets. In this respect, efforts in transporting the radioligands into the cell remains a pressing issue in αSYN PET tracer development.

Data availability statement

Imaging data is available in dicom or text format and can be transferred per request by the corresponding author. Processed data, i.e. %ID/g, αSYN concentrations, data acquired in in vitro binding assays, are available in table format in GraphPad Prism files. Requests for plasmids, or antibody aliquots, should be directed to the corresponding author.

CRediT authorship contribution statement

Sahar Roshanbin: Conceptualization, Methodology, Formal analysis, Investigation, Data curation, Writing – original draft, Supervision, Visualization, Funding acquisition. **Mengfei Xiong:** Conceptualization, Methodology, Formal analysis, Investigation, Data curation, Writing – review & editing. **Greta Hultqvist:** Conceptualization, Methodology, Investigation, Writing – review & editing. **Linda Söderberg:** Methodology, Investigation, Writing – review & editing. **Olof Zachrisson:** Methodology, Resources, Writing – review & editing, Project administration. **Silvio Meier:** Investigation, Writing – review & editing. **Sara Ekmark-Lewén:** Methodology, Investigation, Writing – review & editing. **Joakim Bergström:** Methodology, Writing – review & editing. **Martin Ingelsson:** Methodology, Resources, Writing – review & editing. **Dag Sehlin:** Conceptualization, Methodology, Formal analysis, Investigation, Writing – original draft, Funding acquisition. **Stina Syvänen:** Conceptualization, Methodology, Formal analysis, Investigation, Writing – original draft, Supervision, Project administration, Funding acquisition.

Declaration of competing interest

Linda Söderberg and Olof Zachrisson are employees of BioArctic.

Acknowledgements

We would like to thank AbbVie for providing the sequences for RmAb48, RmAb38F11, RmAb38E2 and RmAb15. We are also grateful to Eliezer Masliah and Philipp Kahle, who developed and characterized the mouse models used. The molecular imaging work in this study was performed at the SciLifeLab Pilot Facility for Preclinical PET-MRI, a Swedish nationally available imaging platform at Uppsala University, Sweden, financed by Knut and Alice Wallenberg Foundation. We also acknowledge BioVis Core Facility/Electron Microscopy at IGP, Uppsala University for assistance with TEM analysis. This work was supported by grants from the Swedish research council (2017–02413, 2018–02715), Alzheimerfonden, Åhlénstiftelsen, Parkinsonfonden, Torsten Söderbergs stiftelse, Hjärnfonden, Konung Gustaf V:S och Drottning Victorias frimurarestiftelse, Major Gösta Linds Minnesfond, Norheds stiftelse, Tore Nilssons stiftelse, O.E. och Edla Johanssons stiftelse and Magnus Bergvalls stiftelse. This project has also received funding from the European Union's Horizon 2020 research and innovation programme under the Marie Skłodowska-Curie grant agreement No 813528. The funding organisations did not take part in the study design, analysis or interpretation of the results.

Appendix A. Supplementary data

Supplementary data to this article can be found online at https://doi.org/10.1016/j.neuropharm.2022.108985.

References

Alafuzoff, I., Libard, S., 2020. Mixed brain pathology is the most common cause of cognitive impairment in the elderly. J. Alzheimers Dis. 78 (1), 453–465.
Appel, L., et al., 2015. Use of 11C-PE2I PET in differential diagnosis of parkinsonian disorders. J. Nucl. Med. 56 (2), 234–242.
Bard, F., et al., 2000. Peripherally administered antibodies against amyloid beta-peptide enter the central nervous system and reduce pathology in a mouse model of Alzheimer disease. Nat. Med. 6 (8), 916–919.
Boado, R.J., et al., 2009. Engineering and expression of a chimeric transferrin receptor monoclonal antibody for blood-brain barrier delivery in the mouse. Biotechnol. Bioeng. 102 (4), 1251–1258.
Burn, D.J., et al., 2006. Motor subtype and cognitive decline in Parkinson's disease, Parkinson's disease with dementia, and dementia with Lewy bodies. J. Neurol. Neurosurg. Psychiatry 77 (5), 585–589.

Chesselet, M.F., et al., 2012. A progressive mouse model of Parkinson's disease: the Thy1-aSyn ("Line 61") mice. Neurotherapeutics 9 (2), 297–314.
Choi, B.K., et al., 2013. Large α-synuclein oligomers inhibit neuronal SNARE-mediated vesicle docking. Proc. Natl. Acad. Sci. U. S. A. 110 (10), 4087–4092.
Clinton, L.K., et al., 2010. Synergistic Interactions between Abeta, tau, and alpha-synuclein: acceleration of neuropathology and cognitive decline. J. Neurosci. 30 (21), 7281–7289.
Compta, Y., et al., 2011. Lewy- and Alzheimer-type pathologies in Parkinson's disease dementia: which is more important? Brain 134 (Pt 5), 1493–1505.
Cummings, J.L., et al., 2011. The role of dopaminergic imaging in patients with symptoms of dopaminergic system neurodegeneration. Brain 134 (Pt 11), 3146–3166.
Danzer, K.M., et al., 2007. Different species of alpha-synuclein oligomers induce calcium influx and seeding. J. Neurosci. 27 (34), 9220–9232.
Deramecourt, V., et al., 2006. Biochemical staging of synucleinopathy and amyloid deposition in dementia with Lewy bodies. J. Neuropathol. Exp. Neurol. 65 (3), 278–288.
Donnemiller, E., et al., 2000. Impaired dopaminergic neurotransmission in patients with traumatic brain injury: a SPECT study using 123I-beta-CIT and 123I-IBZM. Eur. J. Nucl. Med. 27 (9), 1410–1414.
Ekmark-Lewén, S., et al., 2018. Early fine motor impairment and behavioral dysfunction in (Thy-1)-h[A30P] alpha-synuclein mice. Brain Behav. 8 (3), e00915.
Fagerqvist, T., et al., 2013. Monoclonal antibodies selective for α-synuclein oligomers/protofibrils recognize brain pathology in Lewy body disorders and α-synuclein transgenic mice with the disease-causing A30P mutation. J. Neurochem. 126 (1), 131–144.
Fang, X.T., et al., 2017. Efficient and inexpensive transient expression of multispecific multivalent antibodies in Expi293 cells. Biol. Proced. Online 19, 11.
Fang, X.T., et al., 2019. High detection sensitivity with antibody-based PET radioligand for amyloid beta in brain. Neuroimage 184, 881–888.
Faresjö, R., et al., 2021. Brain pharmacokinetics of two BBB penetrating bispecific antibodies of different size. Fluids Barriers CNS 18 (1), 26.
Fodero-Tavoletti, M.T., et al., 2007. In vitro characterization of Pittsburgh compound-B binding to Lewy bodies. J. Neurosci. 27 (39), 10365–10371.
Fodero-Tavoletti, M.T., et al., 2009. In vitro characterisation of BF227 binding to alpha-synuclein/Lewy bodies. Eur. J. Pharmacol. 617 (1–3), 54–58.
Ginovart, N., et al., 1997. PET study of the pre- and post-synaptic dopaminergic markers for the neurodegenerative process in Huntington's disease. Brain 120 (Pt 3), 503–514.
Gustavsson, T., et al., 2020. SPECT imaging of distribution and retention of a brain-penetrating bispecific amyloid-β antibody in a mouse model of Alzheimer's disease. Transl. Neurodegener. 9 (1), 37.
Heise, H., et al., 2005. Molecular-level secondary structure, polymorphism, and dynamics of full-length alpha-synuclein fibrils studied by solid-state NMR. Proc. Natl. Acad. Sci. U. S. A. 102 (44), 15871–15876.
Hultqvist, G., et al., 2017. Bivalent brain shuttle increases antibody uptake by monovalent binding to the transferrin receptor. Theranostics 7 (2), 308–318.
Ingelsson, M., 2016. Alpha-synuclein oligomers-neurotoxic molecules in Parkinson's disease and other Lewy body disorders. Front. Neurosci. 10, 408.
Irwin, D.J., et al., 2017. Neuropathological and genetic correlates of survival and dementia onset in synucleinopathies: a retrospective analysis. Lancet Neurol. 16 (1), 55–65.
Jolly, A.E., et al., 2019. Dopamine D2/D3 receptor abnormalities after traumatic brain injury and their relationship to post-traumatic depression. Neuroimage Clin. 24, 101950.
Kahle, P.J., et al., 2000. Subcellular localization of wild-type and Parkinson's disease-associated mutant alpha -synuclein in human and transgenic mouse brain. J. Neurosci. 20 (17), 6365–6373.
Kariolis, M.S., et al., 2020. Brain delivery of therapeutic proteins using an Fc fragment blood-brain barrier transport vehicle in mice and monkeys. Sci. Transl. Med. 12 (545).
Karpowicz, R.J., et al., 2017. Selective imaging of internalized proteopathic α-synuclein seeds in primary neurons reveals mechanistic insight into transmission of synucleinopathies. J. Biol. Chem. 292 (32), 13482–13497.
Kikuchi, A., et al., 2010. In vivo visualization of alpha-synuclein deposition by carbon-11-labelled 2-[2-(2-dimethylaminothiazol-5-yl)ethenyl]-6-[2-(fluoro)ethoxy]benzoxazole positron emission tomography in multiple system atrophy. Brain 133 (Pt 6), 1772–1778.
Kissel, K., et al., 1998. Immunohistochemical localization of the murine transferrin receptor (TfR) on blood-tissue barriers using a novel anti-TfR monoclonal antibody. Histochem. Cell Biol. 110 (1), 63–72.
Klunk, W.E., et al., 2004. Imaging brain amyloid in Alzheimer's disease with Pittsburgh Compound-B. Ann. Neurol. 55 (3), 306–319.
Kuebler, L., et al., 2020. [11C]MODAG-001-towards a PET tracer targeting α-synuclein aggregates. Eur. J. Nucl. Med. Mol. Imag. 28 (6), 1759–1772.
Lashuel, H.A., et al., 2013. The many faces of α-synuclein: from structure and toxicity to therapeutic target. Nat. Rev. Neurosci. 14 (1), 38–48.
Meier, S.R., et al., 2018. Antibody-based in vivo PET imaging detects amyloid-β reduction in alzheimer transgenic mice after BACE-1 inhibition. J. Nucl. Med. 59 (12), 1885–1891.
Meier, S.R., et al., 2021. Pinpointing brain TREM2 levels in two mouse models of alzheimer's disease. Mol. Imag. Biol.
Moos, T., 1996. Immunohistochemical localization of intraneuronal transferrin receptor immunoreactivity in the adult mouse central nervous system. J. Comp. Neurol. 375 (4), 675–692.
Näsström, T., et al., 2011. The lipid peroxidation products 4-oxo-2-nonenal and 4-hydroxy-2-nonenal promote the formation of α-synuclein oligomers with distinct biochemical, morphological, and functional properties. Free Radic. Biol. Med. 50 (3), 428–437.
Niewoehner, J., et al., 2014. Increased brain penetration and potency of a therapeutic antibody using a monovalent molecular shuttle. Neuron 81 (1), 49–60.
Nordstrom, E., et al., 2011. In: Organization, W.I.P. (Ed.), Protofibril-Binding Antibodies and their use in Therapeutic and Diagnostic Methods for Parkinson's Disease, Dementia with Lewy bodies and other Alpha-Synucleinopathies. US.
Robinson, J.L., et al., 2018. Neurodegenerative disease concomitant proteinopathies are prevalent, age-related and APOE4-associated. Brain 141 (7), 2181–2193.
Rockenstein, E., et al., 2002. Differential neuropathological alterations in transgenic mice expressing alpha-synuclein from the platelet-derived growth factor and Thy-1 promoters. J. Neurosci. Res. 68 (5), 568–578.
Roshanbin, S., et al., 2021. Age-related increase of alpha-synuclein oligomers is associated with motor disturbances in L61 transgenic mice. Neurobiol. Aging 101, 207–220.
Salawu, F.K., Danburam, A., Olokoba, A.B., 2010. Non-motor symptoms of Parkinson's disease: diagnosis and management. Niger. J. Med. 19 (2), 126–131.
Sehlin, D., et al., 2016. Antibody-based PET imaging of amyloid beta in mouse models of Alzheimer's disease. Nat. Commun. 7, 10759.
Sehlin, D., Syvanen, S., faculty, M., 2019. Engineered antibodies: new possibilities for brain PET? Eur. J. Nucl. Med. Mol. Imag. 46 (13), 2848–2858.
Sehlin, D., et al., 2020. Brain delivery of biologics using a cross-species reactive transferrin receptor 1 VNAR shuttle. Faseb. J. 34 (10), 13272–13283.
Shah, M., et al., 2014. Molecular imaging insights into neurodegeneration: focus on α-synuclein radiotracers. J. Nucl. Med. 55 (9), 1397–1400.
Spillantini, M.G., et al., 1997. Alpha-synuclein in Lewy bodies. Nature 388 (6645), 839–840.
Suzuki, M., et al., 2001. Vesicular neurotransmitter transporters in Huntington's disease: initial observations and comparison with traditional synaptic markers. Synapse 41 (4), 329–336.
Syvanen, S., et al., 2017. A bispecific Tribody PET radioligand for visualization of amyloid-beta protofibrils - a new concept for neuroimaging. Neuroimage 148, 55–63.
Syvänen, S., et al., 2018. Efficient clearance of Aβ protofibrils in AβPP-transgenic mice treated with a brain-penetrating bifunctional antibody. Alzheimer's Res. Ther. 10 (1), 49.
Vaikath, N.N., et al., 2015. Generation and characterization of novel conformation-specific monoclonal antibodies for α-synuclein pathology. Neurobiol. Dis. 79, 81–99.
Winner, B., et al., 2011. In vivo demonstration that alpha-synuclein oligomers are toxic. Proc. Natl. Acad. Sci. U. S. A. 108 (10), 4194–4199.
Ye, L., et al., 2008. In vitro high affinity alpha-synuclein binding sites for the amyloid imaging agent PIB are not matched by binding to Lewy bodies in postmortem human brain. J. Neurochem. 105 (4), 1428–1437.
Yu, Y.J., et al., 2011. Boosting brain uptake of a therapeutic antibody by reducing its affinity for a transcytosis target. Sci. Transl. Med. 3 (84), 84ra44.
Yu, L., et al., 2012. Synthesis and in vitro evaluation of α-synuclein ligands. Bioorg. Med. Chem. 20 (15), 4625–4634.
Yu, Y.J., et al., 2014. Therapeutic bispecific antibodies cross the blood-brain barrier in nonhuman primates. Sci. Transl. Med. 6 (261), 261ra154.